Article

Streamflow seasonality in a snow-dwindling world

Juntai Han[1,2,6], Ziwei Liu[1,2,6], Ross Woods[3], Tim R. McVicar[4,5], Dawen Yang[1,2], Taihua Wang[1,2], Ying Hou[1,2], Yuhan Guo[1,2], Changming Li[1,2] & Yuting Yang[1,2✉]

Climate warming induces shifts from snow to rain in cold regions[1], altering snowpack dynamics with consequent impacts on streamflow that raise challenges to many aspects of ecosystem services[2–4]. A straightforward conceptual model states that as the fraction of precipitation falling as snow (snowfall fraction) declines, less solid water is stored over the winter and both snowmelt and streamflow shift earlier in season. Yet the responses of streamflow patterns to shifts in snowfall fraction remain uncertain[5–9]. Here we show that as snowfall fraction declines, the timing of the centre of streamflow mass may be advanced or delayed. Our results, based on analysis of 1950–2020 streamflow measurements across 3,049 snow-affected catchments over the Northern Hemisphere, show that mean snowfall fraction modulates the seasonal response to reductions in snowfall fraction. Specifically, temporal changes in streamflow timing with declining snowfall fraction reveal a gradient from earlier streamflow in snow-rich catchments to delayed streamflow in less snowy catchments. Furthermore, interannual variability of streamflow timing and seasonal variation increase as snowfall fraction decreases across both space and time. Our findings revise the 'less snow equals earlier streamflow' heuristic and instead point towards a complex evolution of seasonal streamflow regimes in a snow-dwindling world.

Snowmelt is a major component of streamflow (Q) in cold regions and serves as an important supply of freshwater resources locally and downstream[2,10], with broad implications for ecosystem functioning[11], food security[4] and natural hazards[12,13]. Observations indicate a substantial warming trend in global cold regions over the past several decades, at a rate much faster than the global average[14], inducing an evident shift of winter precipitation from snowfall towards rainfall[1,15]. This phase change in precipitation is expected to alter the amount, timing and rate of snowpack accumulation and melt[16,17], with profound consequent impacts on the amount and seasonal distribution of Q (refs. 9,18,19). For example, studies in some regions have shown that the annual Q amount may be reduced with declining snowfall fraction (f_s) (ref. 3), possibly owing to more gradual melting of the snowpack and/or higher absorbed net radiation that increases evaporative water loss as a result of snow-albedo feedbacks[16,20].

Compared with the total Q volume, the seasonality of Q is more directly relevant to seasonal water availability[2,4], geomorphology processes[21], reservoir operation[2,10] and flood/drought risks[22,23]. Nonetheless, the responses of Q seasonality to declines in f_s are not yet well understood[9]. In regions where precipitation falls as snow, the discharge of that precipitation as Q can be delayed until the accumulated snow melts in subsequent warmer seasons[4]. It follows that a shift from snowfall towards rainfall is expected to lead to an earlier Q timing, which is supported by earlier snowmelt widely observed across snow-affected regions[5,24,25] and/or by numerical modelling experiments[26,27]. However, direct assessments of Q observations do not always support this expectation[5–8]. Although most existing efforts are made in western North America where the observed Q generally occurs earlier under warming[28–31], relatively less emphasis has been given to other snow-affected regions with limited observational evidence showing diverse trends in Q timing[6,8] (Extended Data Table 1). Moreover, how seasonal variation of Q magnitude responds to declining f_s also remains largely unexplored. Although a few studies have assessed changes in Q seasonal variation in response to climate warming[32], their findings vary considerably among catchments/regions and observational evidence of the direct linkage between f_s and Q seasonal variation remains lacking.

Here we conduct observational analyses to comprehensively assess the impacts of changes in f_s on Q seasonality by using an extensive dataset of long-term (nominally 1950–2020) Q measurements from 3,049 unimpaired, snow-affected (mean annual snowfall fraction higher than 10%) catchments across the Northern Hemisphere (Methods; Extended Data Fig. 1). A fixed water-year from October through to the following September was used for all catchments[33]. Two characteristics of Q seasonality are considered: (1) the timing of Q, represented by the centre of mass of streamflow[34] (CTQ), which denotes the time of year when 50% of the annual Q occurs, and (2) seasonal variation in Q magnitude, characterized by the streamflow concentration index[35] (QCI), whereby a larger QCI value signifies a more pronounced seasonal variation. We also seek to understand how changes in f_s would affect the interannual variability of these two Q seasonality characteristics.

[1]State Key Laboratory of Hydroscience and Engineering, Department of Hydraulic Engineering, Tsinghua University, Beijing, China. [2]Key Laboratory of Hydrosphere Sciences of the Ministry of Water Resources, Beijing, China. [3]School of Civil, Aerospace and Design Engineering, University of Bristol, Bristol, UK. [4]CSIRO Environment, Canberra, New South Wales, Australia. [5]Australian Research Council Centre of Excellence for Climate Extremes, Canberra, New South Wales, Australia. [6]These authors contributed equally: Juntai Han, Ziwei Liu. ✉e-mail: yuting_yang@tsinghua.edu.cn
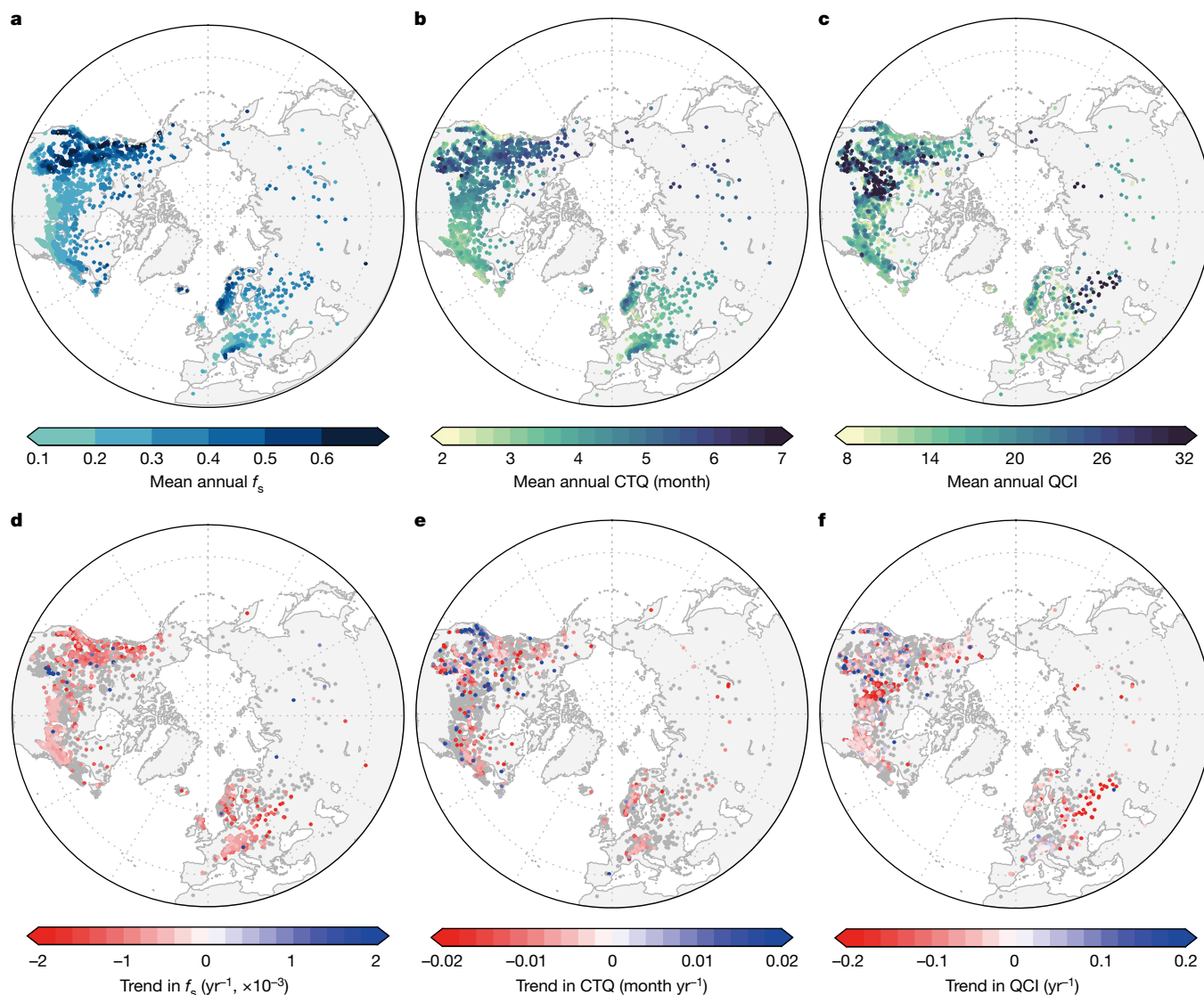
Fig. 1 | Spatiotemporal patterns of snowfall fraction and streamflow seasonality across 3,049 catchments over 1950–2020. a, Spatial distribution of mean annual snowfall fraction. **b**, Spatial distribution of mean annual streamflow timing (represented by CTQ). **c**, Spatial distribution of mean annual seasonal streamflow variation (represented by QCI). **d**, Trends in annual snowfall fraction. **e**, Trends in annual CTQ. **f**, Trends in annual QCI. For **d–f**, grey dots indicate that the trends are not statistically significant ($P > 0.1$, t-test).

Spatial and temporal patterns

To investigate the impacts of changes in f_s on Q seasonality, we first examine the spatial and temporal patterns of f_s and the two Q seasonality indices (CTQ and QCI) for the 3,049 catchments over 1950–2020 (Fig. 1). As shown in Fig. 1a, higher mean annual f_s ($\overline{f_s}$) are generally found in high-mountain regions (for example, the Rocky Mountains and the Alps) and high-latitude areas (for example, northern Europe) (Extended Data Fig. 2). The spatial distributions of mean annual CTQ and QCI broadly follow that of $\overline{f_s}$, with higher $\overline{f_s}$ generally associated with later CTQ and larger QCI, despite a more complex pattern found for QCI (Fig. 1b,c). It is noteworthy that most catchments also exhibit clear precipitation seasonality, with the centre of mass of precipitation (CTP) generally occurring earlier than CTQ in most catchments and more closely matching CTQ in catchments with a lower $\overline{f_s}$ (Fig. 1b and Extended Data Fig. 3). Temporally, widespread declines in f_s are observed over the entire mid-to-high latitude Northern Hemisphere during the past 70 years, with negative annual f_s trends registered in about 85% of the catchments and nearly half of them are statistically significant ($P < 0.1$, t-test) (Fig. 1d). Larger declines in f_s are generally found in catchments with a high $\overline{f_s}$, except for northern Europe where trends in f_s are mostly insignificant. In comparison, trends in annual CTQ show a more diverse pattern with advancing and delaying CTQ trends, respectively, found in about two-thirds and one-third of the catchments (Fig. 1e), suggesting a more intricate response of CTQ to the diminishing f_s over time. Notably, the spatial distribution of CTQ trends does not consistently follow that of CTP either, except for certain regions such as a few catchments in the western United States (Fig. 1e and Extended Data Fig. 3). As for QCI, about 75% of the catchments experienced a decreasing QCI trend, of which about 40% exhibit statistical significance ($P < 0.1$, t-test) (Fig. 1f), implying that historical declines in f_s may have resulted in smaller seasonal Q variation in these catchments.

Snowfall effects on Q seasonality

We subsequently examine the statistical relationships between $\overline{f_s}$ and the two Q seasonality indices across 3,049 catchments to quantify the impact of changes in f_s on Q seasonality. It is found that both CTQ and
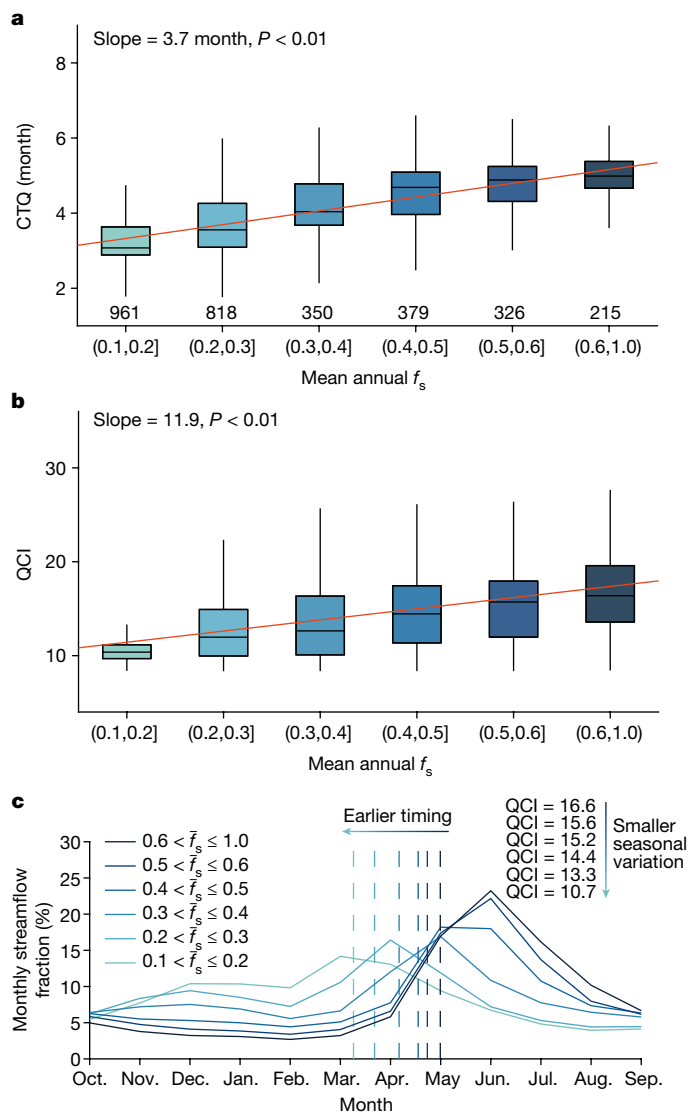
Fig. 2 | Relationship between mean annual snowfall fraction and streamflow seasonality. a, Relationship between mean annual snowfall fraction ($\overline{f_s}$) and mean annual streamflow timing (represented by CTQ) across the 3,049 catchments. **b**, Relationship between mean annual f_s and mean annual streamflow seasonal variation (represented by QCI) across the 3,049 catchments. In **a** and **b**, whiskers represent the 1st and 99th percentile, the top and bottom of the box are the 25th and 75th percentile and the median is represented by the horizontal line internal to the coloured box. The red solid lines show the best linear fit across the 3,049 catchments. **c**, Seasonal course of streamflow for catchments with different $\overline{f_s}$ across the water-year. The 3,049 catchments are stratified into six groups according to their $\overline{f_s}$ (as used in **a** and **b**) and the solid curves represent the mean monthly streamflow series for each group and the vertical dotted lines indicate the mean CTQ in each group. The values of mean QCI for each group are also shown on the right-hand side of this subplot. The number of catchments in each of the six groups is provided at the bottom of **a**.

QCI show a significant ($P < 0.01$, t-test) positive relationship with $\overline{f_s}$, demonstrating that Q in catchments with a higher $\overline{f_s}$ generally occurs later in the year and exhibits a larger seasonal variation (Fig. 2a,b). For catchments with a relatively high $\overline{f_s}$ ($\overline{f_s} > 0.5$), the mean CTQ occurs in around late-April and the mean peak monthly Q occurs in June (Fig. 2c). Moreover, these high-$\overline{f_s}$ catchments are also accompanied by a large seasonal variation in Q (mean QCI > 15), owing to a large contrast between high flows in warmer seasons (the peak monthly Q accounts

for more than 22% of annual Q) and low flows in colder seasons (the minimum monthly Q accounts for less than 3% of annual Q). In comparison, catchments characterized by low $\overline{f_s}$ ($0.1 < \overline{f_s} < 0.2$) manifest both the mean CTQ and peak monthly Q in March. The mean QCI for these low-$\overline{f_s}$ catchments decreased to less than 11, demonstrating a comparatively diminished amplitude of seasonal variations in Q due to the narrower disparity between high- and low-flow during different periods of the year.

The above results in Fig. 2 demonstrate that Q in catchments with a lower $\overline{f_s}$ generally occur earlier and exhibit a smaller seasonal variation. To scrutinize the temporal response of Q seasonality to shifts in f_s, we compared the two streamflow seasonality indices between two 10-year periods with the highest and lowest f_s for individual catchments. The findings show a concordance between the temporal and spatial analyses in terms of the influence of f_s on seasonal Q variation; specifically, the QCI shows greater values during high-f_s periods and comparatively lower values during low-f_s periods (Fig. 3a). This relationship is further illustrated by a positive correlation between trends in QCI and f_s across the 3,049 catchments over 1950–2020 (Extended Data Fig. 4). Notably, the decreased QCI in response to f_s reduction over time is caused primarily by large declines in high flows during warm seasons, whereas the low flows during cold seasons remain essentially unchanged (Fig. 3a and Extended Data Fig. 4).

However, the temporal response of Q timing to changes in f_s does not consistently align with its spatial response and the trends in CTQ do not exhibit a clear relationship with trends in f_s (Extended Data Fig. 4). Nonetheless, the temporal response of Q timing to declines in f_s exhibits a distinct disparity between delayed CTQ in low-$\overline{f_s}$ catchments ($\overline{f_s} < 0.4$) and advanced CTQ in high-$\overline{f_s}$ catchments ($\overline{f_s} > 0.5$) (Fig. 3a). This contrast is further manifested by a clear gradient in the CTQ difference between low- and high-f_s periods: the difference in CTQ between low- and high-f_s periods is mostly positive (indicating a postponed Q timing as f_s decreases) in catchments with a $\overline{f_s} < 0.2$ and becomes increasingly smaller until $\overline{f_s}$ reaches approximately 0.4 to 0.5. After that, a reversal occurs, with the CTQ difference between low- and high-f_s periods turning negative (indicating an earlier Q timing as f_s decreases) and becoming increasingly larger as $\overline{f_s}$ increases (Fig. 3a and Extended Data Fig. 5).

Theoretically, in snow-affected catchments, the timing of Q can be jointly determined by the timing of precipitation and the timing of snowmelt[7,28]. To understand the contrast in the response of CTQ to changes in f_s between low- and high-$\overline{f_s}$ catchments, we explore the responses of CTQ to the timing of precipitation (indicated by CTP) and the initiation of snowmelt (indicated by the melt onset date (MOD)). Two sensitivities, estimated by the slope in the linear regression between CTQ and CTP (ε_{CTQ_CTP}) and between CTQ and MOD (ε_{CTQ_MOD}) for each catchment, are used to quantify the responses of CTQ to CTP and MOD, respectively. We find that ε_{CTQ_CTP} is consistently higher than ε_{CTQ_MOD} in low-$\overline{f_s}$ catchments ($\overline{f_s} < 0.4$) (Fig. 3b and Extended Data Fig. 6), suggesting that the timing of Q in these catchments is controlled primarily by the timing of precipitation. With the increases of $\overline{f_s}$, ε_{CTQ_CTP} decreases whereas ε_{CTQ_MOD} increases and generally surpasses ε_{CTQ_CTP} in high-$\overline{f_s}$ catchments (for example, $\overline{f_s} > 0.5$), indicating the predominant influence of snowmelt on the timing of Q in these high-$\overline{f_s}$ catchments. With this, we further calculate the slope in the linear regression between CTP (MOD) and f_s (that is, ε_{CTP_fs} and ε_{MOD_fs}) to examine the associations of CTP (MOD) with f_s for each catchment (Fig. 3c and Extended Data Fig. 6). As expected, most (about 96%) of catchments exhibit a positive ε_{MOD_fs}, aligning with previous findings that decreased f_s is generally associated with earlier snowmelt[5,23]. The positive MOD–f_s relationship and a higher ε_{CTQ_MOD} jointly led to an advancement in CTQ as f_s diminished in high-$\overline{f_s}$ catchments. As for CTP, a negative ε_{CTP_fs} is found in nearly all catchments (about 98%), indicating that a decline in f_s is also commonly associated with, or more likely contributed by, a delay in seasonal precipitation (due to reduced cold
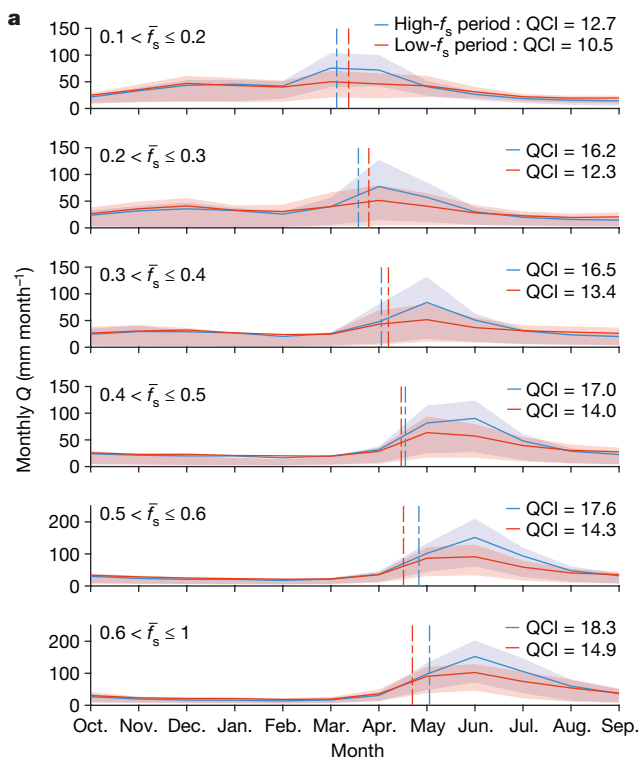
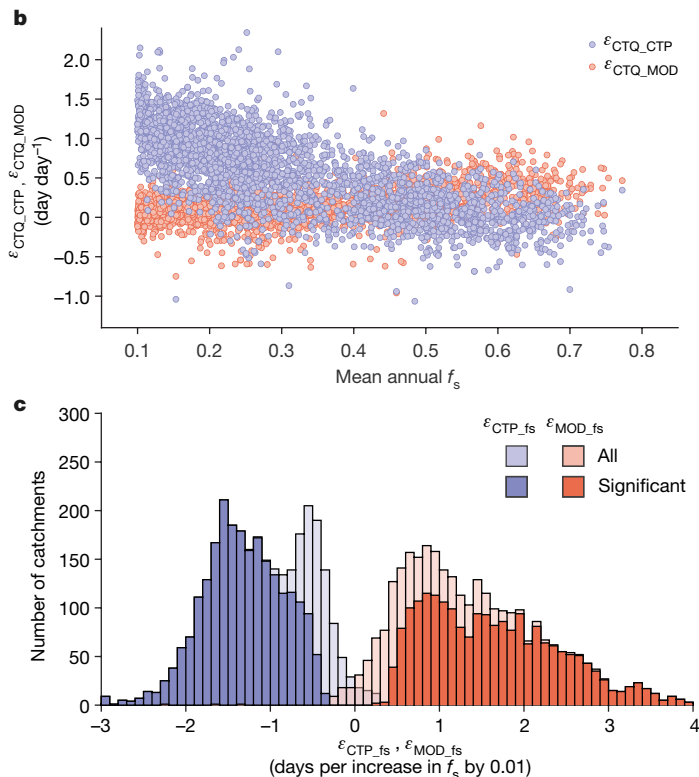**Fig. 3 | Impacts of temporal changes in snowfall fraction on streamflow seasonality. a**, Comparison of mean monthly streamflow over the water-year between the two 10-year periods with the highest (blue) and lowest (red) snowfall fractions for each six groups of catchments. The 3,049 catchments are first divided into six groups according to their mean annual snow fraction ($\overline{f_s}$). Then for each catchment in each group, the two extreme f_s 10-year periods are identified which are then averaged for each group. Solid curves represent the mean of all catchments and shadow areas represent the range of individual catchments in each group. The vertical lines indicate the streamflow timing

(represented by CTQ) and the seasonal variation of streamflow (represented by QCI) is also shown. **b**, Sensitivities of CTQ to precipitation timing (ε_{CTQ_CTP}) and melt onset date (ε_{CTQ_MOD}), which, respectively, quantify the impact of one-day change in CTP and MOD on CTQ, as a function of $\overline{f_s}$ for the 3,049 catchments. **c**, Histogram of slopes in the linear regressions between precipitation timing (melt onset date) and snowfall fraction (ε_{CTP_fs} and ε_{MOD_fs}), which, respectively, quantify changes in CTP and MOD in relation to increases in f_s by 0.01, for the 3,049 catchments.

season precipitation; Extended Data Fig. 7). This negative CTP–f_s relationship, along with a higher ε_{CTQ_CTP}, collectively contributed to a delayed CTQ following decreases in f_s in low-$\overline{f_s}$ catchments ($\overline{f_s}$ less than about 0.4).

Variability of Q seasonality

To demonstrate how changes in f_s alter the interannual variability of Q seasonality, we first calculate the coefficient of variation of annual CTQ (CV$_{CTQ}$) and QCI (CV$_{QCI}$) over the entire data period for each catchment. Moreover, because the interannual variability of Q can be considerably influenced by that of precipitation, we also calculate the corresponding indices for precipitation (CV$_{CTP}$ and CV$_{PCI}$). We then classify the 3,049 catchments into three groups based on CV$_{CTP}$ (or CV$_{PCI}$) and examine how CV$_{CTQ}$ and CV$_{QCI}$ vary with $\overline{f_s}$ across catchments in each group. Results show that for the same $\overline{f_s}$, catchments with higher CV$_{CTP}$ (CV$_{PCI}$) generally show higher CV$_{CTQ}$ (CV$_{QCI}$), confirming a critical role of precipitation in governing the interannual variability of Q seasonality (Fig. 4a,b). Meanwhile, we find that both CV$_{CTQ}$ and CV$_{QCI}$ exhibit a significant ($P < 0.01$, t-test) negative relationship with $\overline{f_s}$ for all three catchment groups, indicating larger interannual variability of Q timing and seasonal variation in catchments with lower $\overline{f_s}$ for a given CV$_{CTP}$ and CV$_{PCI}$.

To further investigate how CV$_{CTQ}$ and CV$_{QCI}$ change with f_s through time, we adopt a 20-year moving window and examine the relationships between relative changes in CV$_{CTQ}$ (CV$_{QCI}$) and CV$_{CTP}$ (CV$_{PCI}$) between the two 20-year periods with the highest and lowest f_s for each

catchment. The 20-year window was selected to ensure the sample size was long enough to account for interannual variability. Results show that the sensitivities of CV$_{CTQ}$ (CV$_{QCI}$) to CV$_{CTP}$ (CV$_{PCI}$) evidently increase as $\overline{f_s}$ decreases (Fig. 4c,d). This means that the interannual variability of precipitation seasonality exerted a stronger control on the interannual variability of Q seasonality as f_s decreases. Comparison of the sensitivities of CV$_{CTQ}$ (CV$_{QCI}$) to CV$_{CTP}$ (CV$_{PCI}$) among catchments experiencing different f_s changes also shows a similar finding (Extended Data Fig. 8), because changes in f_s are largely related to the magnitude of f_s (Fig. 1a,d). This result implies that when the interannual variability of precipitation seasonality remains unchanged, decreases in f_s would increase the variability of Q timing and seasonal variation between years, consistent with findings from the spatial analyses (Fig. 4a,b).

Summary and discussion

Although it has long been recognized that warming-induced declines in snowfall will exert profound impacts on Q characteristics, the underlying mechanisms are complex and existing findings vary substantially across geographic locations[5,8,9,26]. Here, by using long-term Q observations across many catchments over the entire Northern Hemisphere, we present a comprehensive observation-based assessment of the impacts of changes in f_s on Q seasonality. Three key conclusions are obtained.

First, seasonal Q variation decreases with the decline in f_s. This response is consistent across both space and time and is caused by a decreased warm season fractional Q and an increased cold season fractional Q, consistent with previous findings[36–38]. However, when
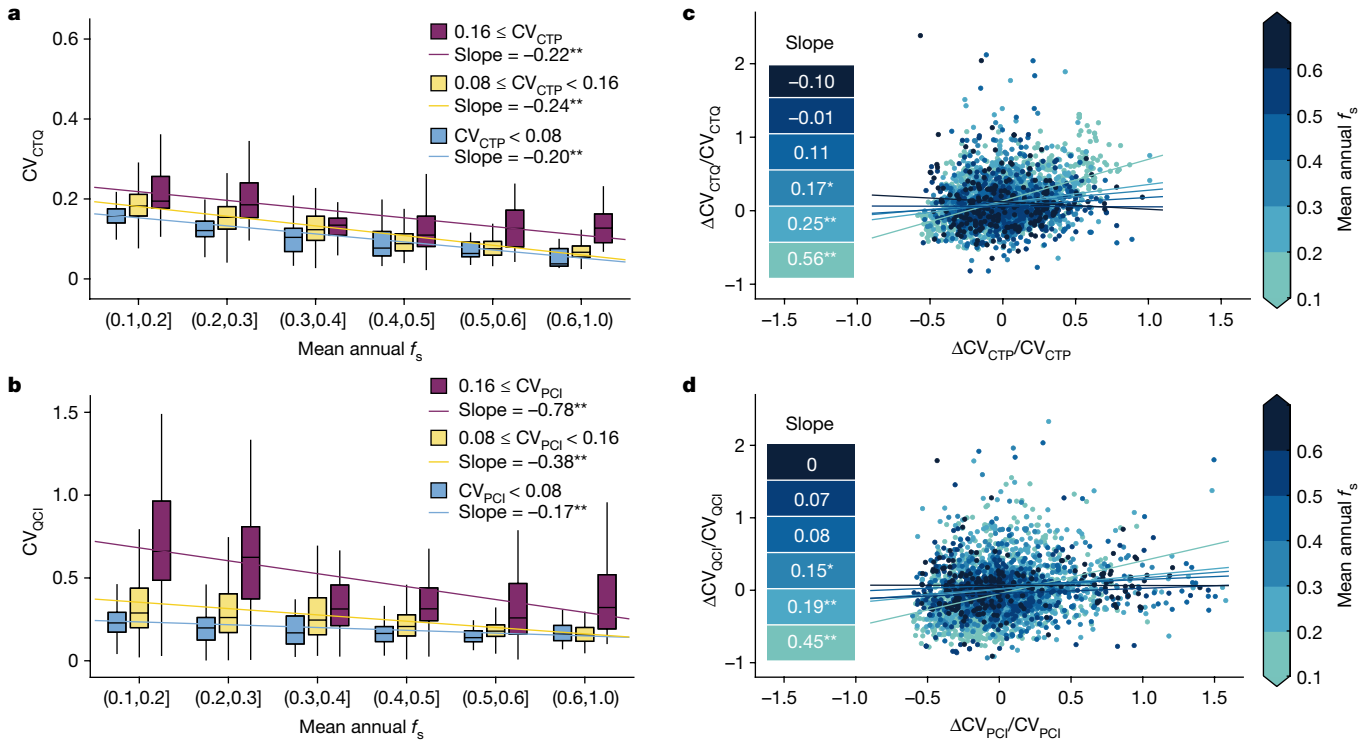
Fig. 4 | Impacts of declines in snowfall fraction on the interannual variability of streamflow seasonality. a, Relationship between interannual variability of streamflow timing (CV_{CTQ}) and mean annual snowfall fraction ($\overline{f_s}$) across the 3,049 catchments. **b**, Relationship between interannual variability of seasonal streamflow variation (CV_{QCI}) and $\overline{f_s}$ across the 3,049 catchments. In **a** and **b**, whiskers represent the 1st and 99th percentile, the top and bottom of the box are the 25th and 75th percentile and the median is represented by the horizontal line internal to the coloured box. The solid lines show the best linear fit across the 3,049 catchments with the slope and probability level (calculated by means of a *t*-test) shown in the legend for the three groups. **c**, Relationship of relative change in interannual variability of streamflow timing ($\Delta CV_{CTQ}/CV_{CTQ}$) and that of precipitation timing ($\Delta CV_{CTP}/CV_{CTP}$) between two 20-year periods with the highest and lowest f_s. **d**, Relationship of relative change in interannual variability of streamflow seasonal variation ($\Delta CV_{QCI}/CV_{QCI}$) and that of precipitation seasonal variation ($\Delta CV_{PCI}/CV_{PCI}$) between two 20-year periods with the highest and lowest f_s. In **c** and **d**, catchments are divided into six groups on the basis of their $\overline{f_s}$, and lines are the best linear fit across catchments in each group. The slopes of the linear regression models are presented in the inset, denoted by asterisks * and ** to signify statistical significance at the 95% and 99% confidence levels (*t*-test), respectively.

absolute *Q* changes are assessed, the warm season *Q* shows an evident reduction whereas the cold season *Q* remains relatively stable (Fig. 3a and Extended Data Fig. 7), implying that the annual total *Q* must decrease as f_s declines[3]. Consequently, the increased cold season fractional *Q* is driven primarily by decreases in annual total *Q* rather than increases in cold season *Q* itself. The decreased warm season *Q* can be directly attributed to a reduced water supply from snowmelt[30] and potentially amplified evaporation losses as a result of enhanced energy availability[20]. Mechanisms underlying changes in cold season *Q* are more complex. Although the intuitive notion is that rainfall directly generates runoff so that a shift from snow toward rain will increase cold season *Q* (ref. 2), our results show that a decline in f_s is commonly associated with a delayed seasonal precipitation (Fig. 3c), which implies a decreased cold season precipitation (Extended Data Fig. 7). Additionally, enhanced evaporation and decreased snowmelt rate are also likely to reduce cold season *Q* (refs. 16,18). Collectively, these opposing effects seem to have substantially offset each other, yielding marginal net changes in cold season *Q*.

Second, declines in f_s do not always lead to an earlier *Q* timing. Although most existing observational evidence indicates an earlier *Q* timing due to earlier snowmelt associated with declines in f_s under warming, these previous findings are mostly concentrated in western North America where $\overline{f_s}$ is relatively high[28–31,39]. By extending existing analyses to the entire Northern Hemisphere, our results demonstrate that the lower f_s to earlier *Q* relationship generally persists spatially but does not always hold over time. Specifically, advances in seasonal *Q* are found mostly in catchments with a relatively high $\overline{f_s}$, consistent

with previous findings in western North America. By contrast, delays in seasonal *Q* are observed in catchments with relatively lower $\overline{f_s}$, which is driven primarily by delays in seasonal precipitation despite earlier snowmelt as f_s decreases.

Moreover, as $\overline{f_s}$ generally increases with elevation, discernible contrasts in the alterations of seasonal *Q* timing with declining f_s are similarly observed along an elevation gradient, showing advanced (delayed) seasonal *Q* predominantly in catchments at higher (lower) elevations (Extended Data Fig. 5). This is expected and hints at an elevation dependence of changes in *Q* timing with declining f_s. Previous studies reported that snowpack dynamics are more sensitive to temperature changes at lower elevations and more responsive to precipitation changes at higher elevations[40–42]. Here we observe that ε_{CTP_fs} becomes more negative whereas ε_{MOD_fs} becomes less positive as elevation increases (Extended Data Fig. 9). Because MOD is largely controlled by temperature (or more precisely energy availability[24]), this result indicates that changes in f_s are more closely associated with changes in precipitation and less so with changes in temperature as elevation increases, consistent with previous findings on snowpack dynamics. Furthermore, by multiplying the changes in CTP and MOD (ΔCTP and ΔMOD) with the dependence of *Q* timing on CTP and MOD (ε_{CTQ_CTP} and ε_{CTQ_CTP}, as shown in Fig. 3b), we can approximately estimate the impact of ΔCTP and ΔMOD on ΔCTQ, respectively. Results show that ΔCTP-induced ΔCTQ becomes increasingly less positive, whereas ΔMOD-induced ΔCTQ becomes increasingly negative with rising elevation (Extended Data Fig. 9). These trends combine to result in the ΔCTQ gradient from advanced CTQ in high-$\overline{f_s}$ (high-elevation) catchments

Article

to delayed CTQ in low-$\overline{f_s}$ (low-elevation) catchments (Fig. 3a and Extended Data Fig. 5). Notably, a reversal in ΔCTQ (from advancing to delaying) between high- and low-f_s periods generally occurs when $\overline{f_s}$ approximates 0.4, corresponding to an elevation of about 1,500 m. This suggests a critical $\overline{f_s}$ and elevation threshold influencing the composition of Q regimes, distinguishing between snowmelt-dominated and rainfall-dominated Q regimes[41]. Intriguingly, this critical elevation threshold on Q timing changes aligns reasonably well with previous findings about the critical elevation that distinguishes temperature-dominated from precipitation-dominated controls on snowpack dynamics (for example, about 1,560 m in the Central Rocky Mountains[42] and about 1,400 m in the Alps[43]). With ongoing climatic warming, this critical elevation governing climatic controls of snowpack dynamics was projected to rise in the future[44]. In this context, it remains of interest to assess whether similar shifts would manifest in the $\overline{f_s}$ and elevation thresholds for changes in Q timing and runoff-generation regime under future warming.

Third, declines in f_s increase the interannual variability of streamflow seasonality. We found that the interannual variability of CTQ and QCI become larger and are increasingly controlled by CTP and PCI as f_s decreases across both space and time (Fig. 4 and Extended Data Fig. 8). Although the interannual variability of Q is widely recognized as being defined primarily by the interannual variability of precipitation[45], we demonstrated that higher precipitation variability does not necessarily lead to a higher Q variability due to the presence of snow. When f_s is high, the interannual variability of seasonal Q timing and variation are more controlled by that of snowmelt, which is determined primarily by the interannual variability of energy supply that is usually much smaller than the interannual variability of precipitation[46]. This pinpoints an important buffering role of snow in mediating the partitioning of precipitation variance into Q variance[45], which, however, is weakening as f_s diminishes with ongoing climate warming. Meanwhile, climate models project that the interannual variability of global mean land precipitation will increase at a rate of 4–5% per degree increase in temperature[47], suggesting that the interannual variability of Q seasonality will be further amplified under future warming.

The above findings on the responses of streamflow seasonality to declines in f_s have important hydrologic implications. Although previous studies concluded that earlier snowmelt would increase the risk of spring flood[48], our results indicate that the frequency of spring flood might increase primarily in high-$\overline{f_s}$ catchments, whereas fewer spring floods may be expected in catchments where $\overline{f_s}$ is relatively lower. Furthermore, subtle changes in cold season Q coupled with substantial declines in warm season Q imply a decreased magnitude of snowmelt floods as f_s declines—a phenomenon that has already been globally documented in the assessments of river flood changes[49]. By contrast, decreased warm season Q directly indicates a higher risk of summer and/or autumn drought, potentially exerting adverse effects on broad aspects of water/food security[4], ecosystem health[11] and hydropower generation[2]. Meanwhile, the increased interannual variability of Q seasonality implies a higher uncertainty in the seasonal Q regime, which results in larger difficulties in predicting seasonal Q changes thereby posing further challenges to seasonal and interannual water resources planning and management. In this light, adaptive measures, for example, seeking alternative water supplies (groundwater), increasing reservoir capacities and/or increasing the efficiency of water use, are imperative to enhance the resilience of the water system against dwindling f_s to maintain ecosystem service functions in snow-affected and downstream regions under future warming.

Online content

Any methods, additional references, Nature Portfolio reporting summaries, source data, extended data, supplementary information, acknowledgements, peer review information; details of author contributions and competing interests; and statements of data and code availability are available at https://doi.org/10.1038/s41586-024-07299-y.

1. Bintanja, R. & Andry, O. Towards a rain-dominated Arctic. *Nat. Clim. Change* **7**, 263–267 (2017).
2. Barnett, T. P., Adam, J. C. & Lettenmaier, D. P. Potential impacts of a warming climate on water availability in snow-dominated regions. *Nature* **438**, 303–309 (2005).
3. Berghuijs, W. R., Woods, R. A. & Hrachowitz, M. A precipitation shift from snow towards rain leads to a decrease in streamflow. *Nat. Clim. Change* **4**, 583–586 (2014).
4. Qin, Y. et al. Agricultural risks from changing snowmelt. *Nat. Clim. Change* **10**, 459–465 (2020).
5. Fritze, H., Stewart, I. T. & Pebesma, E. Shifts in western North American snowmelt runoff regimes for the recent warm decades. *J. Hydrometeorol.* **12**, 989–1006 (2011).
6. Wasko, C., Nathan, R. & Peel, M. C. Trends in global flood and streamflow timing based on local water year. *Water Resour. Res.* **56**, e2020WR027233 (2020).
7. Shi, X., Marsh, P. & Yang, D. Warming spring air temperatures, but delayed spring streamflow in an Arctic headwater basin. *Environ. Res. Lett.* **10**, 064003 (2015).
8. Uzun, S. et al. Changes in snowmelt runoff timing in the contiguous United States. *Hydrol. Process.* **35**, e14430 (2021).
9. Gordon, B. L. et al. Why does snowmelt-driven streamflow response to warming vary? A data-driven review and predictive framework. *Environ. Res. Lett.* **17**, 053004 (2022).
10. Siirila-Woodburn, E. R. et al. A low-to-no snow future and its impacts on water resources in the western United States. *Nat. Rev. Earth .Environ.* **2**, 800–819 (2021).
11. Slatyer, R. A., Umbers, K. D. L. & Arnold, P. A. Ecological responses to variation in seasonal snow cover. *Conserv. Biol.* **36**, e13727 (2022).
12. Livneh, B. & Badger, A. M. Drought less predictable under declining future snowpack. *Nat. Clim. Change* **10**, 452–458 (2020).
13. Ombadi, M., Risser, M. D., Rhoades, A. M. & Varadharajan, C. A warming-induced reduction in snow fraction amplifies rainfall extremes. *Nature* **619**, 305–310 (2023).
14. Mu, C. et al. The status and stability of permafrost carbon on the Tibetan Plateau. *Earth Sci. Rev.* **211**, 103433 (2020).
15. Knowles, N., Dettinger, M. D. & Cayan, D. R. Trends in snowfall versus rainfall in the western United States. *J. Clim.* **19**, 4545–4559 (2006).
16. Musselman, K. N., Clark, M. P., Liu, C., Ikeda, K. & Rasmussen, R. Slower snowmelt in a warmer world. *Nat. Clim. Change* **7**, 214–219 (2017).
17. Smith, T. & Bookhagen, B. Changes in seasonal snow water equivalent distribution in High Mountain Asia (1987 to 2009). *Sci. Adv.* **4**, e1701550 (2018).
18. Barnhart, T. B. et al. Snowmelt rate dictates streamflow. *Geophys. Res. Lett.* **43**, 8006–8016 (2016).
19. Musselman, K. N., Addor, N., Vano, J. A. & Molotch, N. P. Winter melt trends portend widespread declines in snow water resources. *Nat. Clim. Change* **11**, 418–424 (2021).
20. Milly, P. C. D. & Dunne, K. A. Colorado River flow dwindles as warming-driven loss of reflective snow energizes evaporation. *Science* **367**, 1252–1255 (2020).
21. Church, M. Geomorphic thresholds in riverine landscapes. *Freshw. Biol.* **47**, 541–557 (2002).
22. Brunner, M. I., Slater, L., Tallaksen, L. M. & Clark, M. Challenges in modeling and predicting floods and droughts: a review. *WIREs Water* **8**, e1520 (2021).
23. Blahušiaková, A. et al. Snow and climate trends and their impact on seasonal runoff and hydrological drought types in selected mountain catchments in Central Europe. *Hydrol. Sci. J.* **65**, 2083–2096 (2020).
24. Clow, D. W. Changes in the timing of snowmelt and streamflow in Colorado: a response to recent warming. *J. Clim.* **23**, 2293–2306 (2010).
25. Cayan, D. R., Kammerdiener, S. A., Dettinger, M. D., Caprio, J. M. & Peterson, D. H. Changes in the onset of spring in the western United States. *Bull. Am. Meteorol. Soc.* **82**, 399–415 (2001).
26. McCabe, G. J., Wolock, D. M. & Valentin, M. Warming is driving decreases in snow fractions while runoff efficiency remains mostly unchanged in snow-covered areas of the western United States. *J. Hydrometeorol.* **19**, 803–814 (2018).
27. Kiewiet, L. et al. Effects of spatial and temporal variability in surface water inputs on streamflow generation and cessation in the rain–snow transition zone. *Hydrol. Earth Syst. Sci.* **26**, 2779–2796 (2022).
28. Aguado, E., Cayan, D., Riddle, L. & Roos, M. Climatic fluctuations and the timing of west coast streamflow. *J. Clim.* **5**, 1468–1483 (1992).
29. McCabe, G. J. & Clark, M. P. Trends and variability in snowmelt runoff in the western United States. *J. Hydrometeorol.* **6**, 476–482 (2005).
30. Stewart, I. T., Cayan, D. R. & Dettinger, M. D. Changes toward earlier streamflow timing across western North America. *J. Clim.* **18**, 1136–1155 (2005).
31. Pederson, G. T. et al. Climatic controls on the snowmelt hydrology of the northern Rocky Mountains. *J. Clim.* **24**, 1666–1687 (2011).
32. Eisner, S. et al. An ensemble analysis of climate change impacts on streamflow seasonality across 11 large river basins. *Clim. Change* **141**, 401–417 (2017).
33. *Water Year: Glossary of Meteorology* (American Meteorological Society, 2012).
34. Court, A. Measures of streamflow timing. *J. Geophys. Res.* **67**, 4335–4339 (1962).
35. Oliver, J. E. Monthly precipitation distribution: a comparative index. *Profess. Geogr.* **32**, 300–309 (1980).
36. Jefferson, A. J. Seasonal versus transient snow and the elevation dependence of climate sensitivity in maritime mountainous regions. *Geophys. Res. Lett.* **38**, L16402 (2011).
37. Nayak, A., Marks, D., Chandler, D. G. & Seyfried, M. Long-term snow, climate and streamflow trends at the Reynolds Creek Experimental Watershed, Owyhee Mountains, Idaho, United States. *Water Resour. Res.* **46**, W06519 (2010).
38. Stewart, I. T. Changes in snowpack and snowmelt runoff for key mountain regions. *Hydrol. Process.* **23**, 78–94 (2009).
39. Dettinger, M. D. & Cayan, D. R. Large-scale atmospheric forcing of recent trends toward early snowmelt runoff in California. *J. Clim.* **8**, 606–623 (1995).
40. Mote, P. W., Hamlet, A. F., Clark, M. P. & Lettenmaier, D. P. Declining mountain snowpack in western North America. *Bull. Am. Meteorol. Soc.* **86**, 39–49 (2005).

41. Li, D., Wrzesien, M. L., Durand, M., Adam, J. & Lettenmaier, D. P. How much runoff originates as snow in the western United States and how will that change in the future? *Geophys. Res. Lett.* **44**, 6163–6172 (2017).

42. Sospedra-Alfonso, R., Melton, J. R. & Merryfield, W. J. Effects of temperature and precipitation on snowpack variability in the Central Rocky Mountains as a function of elevation. *Geophys. Res. Lett.* **42**, 4429–4438 (2015).

43. Morán-Tejeda, E., Ignacio López-Moreno, J. & Beniston, M. The changing roles of temperature and precipitation on snowpack variability in Switzerland as a function of altitude. *Geophys. Res. Lett.* **40**, 2131–2136 (2013).

44. Scalzitti, J., Strong, C. & Kochanski, A. Climate change impact on the roles of tempearture and precipitation in western U.S. snowpack variability. *Geophys. Res. Lett.* **43**, 5361–5369 (2013).

45. Yin, D. & Roderick, M. L. Inter-annual variability of the global terrestrial water cycle. *Hydrol. Earth Syst. Sci.* **24**, 381–396 (2020).

46. McMahon, T. A., Peel, M. C., Pegram, G. G. S. & Smith, I. N. A simple methodology for estimating mean and variability of annual runoff and reservoir yield under present and future climates. *J. Hydrometeorol.* **12**, 135–146 (2011).

47. Pendergrass, A. G., Knutti, R., Lehner, F., Deser, C. & Sanderson, B. M. Precipitation variability increases in a warmer climate. *Sci. Rep.* **7**, 17966 (2017).

48. Allamano, P., Claps, P. & Laio, F. Global warming increases flood risk in mountainous areas. *Geophys. Res. Lett.* **36**, L24404 (2009).

49. Zhang, S. et al. Reconciling disagreement on global river flood changes in a warming climate. *Nat. Clim. Change* **12**, 1160–1167 (2022).

Article

Methods

Datasets

We use daily and/or monthly measurements of streamflow (Q) from 3,049 catchments (including their boundaries), sourced from four global/regional Q databases, including the following: (1) the Global Runoff Data Centre, Germany (https://www.bafg.de/GRDC/EN/01_GRDC/grdc_node.html); (2) the USGS National Water Information System (https://waterdata.usgs.gov/nwis/sw); (3) European Water Archive of EURO-FRIEND-Water (https://www.bafg.de/GRDC/EN/04_spcldtbss/42_EWA/ewa_node.html); and (4) the Water Survey of Canada Hydrometric Data (https://wateroffice.ec.gc.ca/). The selected 3,049 catchments all satisfy the following four criteria. First, the catchments had at least 30 years of continuous Q records over 1950–2020, with a maximum data gap of 10 days; the remaining gaps were then filled using linear interpolation. Second, to minimize the influence of human interventions, all catchments had irrigation areas smaller than 3% of the catchment area (based on the Global Map of Irrigation Areas-GMIA[50]), urban areas smaller than 1% of the catchment area (based on the GlobCover v.2.3 map[51]) and reservoir capacities smaller than 3% of the mean annual Q (based on the Global Reservoir and Dam database[52]). Third, to focus on the snow impact, all catchments had a mean annual snowfall fraction (the ratio of snowfall over precipitation) higher than 10%. Fourth and finally, catchments in the Southern Hemisphere were excluded to ensure a consistent water-year for all analysed catchments. A fixed water-year (1 October through 30 September of the following calendar year[53]) was used for all catchments. It should be noted that the Q database is temporally heterogeneous. Despite that, the catchments collectively encompass about 45% of the snow-affected regions over the entire Northern Hemisphere with the lengths of Q records varying from 30 to 70 years (mean is about 55 years) (Extended Data Fig. 1).

Hourly precipitation, net radiation, snowfall and snow water equivalent (SWE) at 0.1° spatial resolution over 1950–2020 were obtained from the fifth generation of European ReAnalysis (ERA5-Land) dataset[53]. The gridded data were further spatially lumped for each catchment and temporally aggregated to daily and/or monthly scales. The ERA5-Land dataset features long temporal coverage and high spatial resolution and has undergone rigorous evaluation against observations, which confirms its accuracy and suitability for long-term hydrological investigations[13,53].

Summary of calculations

To quantify the Q seasonality, we adopt two Q indices to, respectively, determine the timing and seasonal variation of Q. Specifically, CTQ[34] is used to indicate the seasonal Q timing, which denotes the time of year when 50% of the annual streamflow occurs and is calculated as:

$$\text{CTQ} = \sum_{i=1}^{12} (i \times q_i) / \sum_{i=1}^{12} (q_i) \tag{1}$$

where i is time in months from the beginning of the water-year and q_i is monthly Q (mm month^{-1}) for water-year month i.

The QCI[35] is used to quantify the seasonal variation of Q and is calculated as:

$$\text{QCI} = \sum_{i=1}^{12} q_i^2 / \left(\sum_{i=1}^{12} q_i \right)^2 \times 100 \tag{2}$$

The two Q indices have been widely used in the literature to assess Q and/or P seasonality characteristics under global change[30,54] (Extended Data Table 1). To account for the influence of changing precipitation, we similarly calculated the corresponding indices for precipitation (CTP and PCI) in the same way.

The MOD is determined as the first date in the water-year when SWE starts to drop after reaching the maximum SWE[24]. Adopting a different definition of SWE yields similar results (Extended Data Fig. 6). The period between MOD and the first date SWE starts to increase is defined as the warm season and the rest of the year is considered as the cold season. In the assessment of changes in seasonal precipitation and Q, the climatological warm season and cold season were used for each catchment, which are determined from the mean annual daily courses of SWE.

Data availability

The hourly ERA5-Land data are available from the Copernicus Climate Change Service (C3S) Climate Date Store at https://cds.climate.copernicus.eu/cdsapp#!/dataset/reanalysis-era5-land?tab=overview. Streamflow data are available from four sources: (1) the Global Runoff Data Centre (https://www.bafg.de/GRDC/EN/01_GRDC/grdc_node.html); (2) the USGS National Water Information System (https://waterdata.usgs.gov/nwis/sw); (3) European Water Archive of EURO-FRIEND-Water (https://www.bafg.de/GRDC/EN/04_spcldtbss/42_EWA/ewa_node.html); and (4) the Water Survey of Canada Hydrometric Data (https://wateroffice.ec.gc.ca/). Metadata for the 3,049 catchments used in the analysis are available at https://doi.org/10.5281/zenodo.10692562 (ref. 55). Map figures were created using Natural Earth Data included in the MATLAB software. Source data are provided with this paper.

Code availability

Analyses presented here do not depend on specific code; the approach can be reproduced following the procedures described in the Methods.

50. Siebert, S. et al. A global data set of the extent of irrigated land from 1900 to 2005. *Hydrol. Earth Syst. Sci.* **19**, 1521–1545 (2015).
51. Arino O., Ramos, J., Kalogirou, V., Defourny, P. & Achard, F. GlobCover 2009. In *ESA Living Planet Symposium, 27 June* https://epic.awi.de/id/eprint/31046/1/Arino_et_al_GlobCover2009-a.pdf (2 July 2010).
52. Lehner, B. et al. High-resolution mapping of the world's reservoirs and dams for sustainable river-flow management. *Front. Ecol. Environ.* **9**, 494–502 (2011).
53. Muñoz-Sabater, J. et al. ERA5-Land: a state-of-the-art global reanalysis dataset for land applications. *Earth Syst. Sci. Data* **13**, 4349–4383 (2021).
54. Sloat, L. L. et al. Increasing importance of precipitation variability on global livestock grazing lands. *Nat. Clim. Change* **8**, 214–218 (2018).
55. Han, J. et al. Metadata for the 3049 catchments. *Zenodo* https://zenodo.org/records/10692562 (2024).
56. Lettenmaier, D. P. & Gan, T. Y. Hydrologic sensitivities of the Sacramento-San Joaquin River Basin, California, to global warming. *Water Resour. Res.* **26**, 69–86 (1990).
57. Nash, L. L. & Gleick, P. H. Sensitivity of streamflow in the Colorado Basin to climatic changes. *J. Hydrol.* **125**, 221–241 (1991).
58. Jeton, A. E., Dettinger, M. D. & Smith, J. L. *Potential Effects of Climate Change on Streamflow, Eastern and Western Slopes of the Sierra Nevada, California and Nevada* Water-Resources Investigations Report 95-4260 (USGS, 1996).
59. Yang, D. et al. Siberian Lena River hydrologic regime and recent change. *J. Geophys. Res. Atmos.* **107**, ACL14-1–ACL14-10 (2002).
60. Dettinger, M. D., Cayan, D. R., Meyer, M. K. & Jeton, A. E. Simulated hydrologic responses to climate variations and change in the Merced, Carson and American River Basins, Sierra Nevada, California, 1900–2099. *Clim. Change* **62**, 283–317 (2004).
61. Jasper, K., Calanca, P., Gyalistras, D. & Fuhrer, J. Differential impacts of climate change on the hydrology of two alpine river basins. *Clim. Res.* **26**, 113–129 (2004).
62. Regonda, S. K., Rajagopalan, B., Clark, M. & Pitlick, J. Seasonal cycle shifts in hydroclimatology over the western United States. *J. Clim.* **18**, 372–384 (2005).
63. Zierl, B. & Bugmann, H. Global change impacts on hydrological processes in Alpine catchments. *Water Resour. Res.* **41**, W02028 (2005).
64. Hodgkins, G. A. & Dudley, R. W. Changes in the timing of winter–spring streamflows in eastern North America, 1913–2002. *Geophys. Res. Lett.* **33**, L06402 (2006).
65. Hamlet, A. F., Mote, P. W., Clark, M. P. & Lettenmaier, D. P. Twentieth-century trends in runoff, evapotranspiration and soil moisture in the western United States. *J. Clim.* **20**, 1468–1486 (2007).
66. Moore, J. N., Harper, J. T. & Greenwood, M. C. Significance of trends toward earlier snowmelt runoff, Columbia and Missouri Basin headwaters, western United States. *Geophys. Res. Lett.* **34**, L16402 (2007).
67. Yang, D., Zhao, Y., Armstrong, R., Robinson, D. & Brodzik, M.-J. Streamflow response to seasonal snow cover mass changes over large Siberian watersheds. *J. Geophys. Res. Earth Surf.* **112**, F02S22 (2007).
68. Burn, D. H. Climatic influences on streamflow timing in the headwaters of the Mackenzie River Basin. *J. Hydrol.* **352**, 225–238 (2008).
69. Hidalgo, H. G. et al. Detection and attribution of streamflow timing changes to climate change in the western United States. *J. Clim.* **22**, 3838–3855 (2009).

70. Godsey, S. E., Kirchner, J. W. & Tague, C. L. Effects of changes in winter snowpacks on summer low flows: case studies in the Sierra Nevada, California, USA. *Hydrol. Process.* **28**, 5048–5064 (2014).
71. Morán-Tejeda, E., Lorenzo-Lacruz, J., López-Moreno, J. I., Rahman, K. & Beniston, M. Streamflow timing of mountain rivers in Spain: recent changes and future projections. *J. Hydrol.* **517**, 1114–1127 (2014).
72. Burn, D. H. & Whitfield, P. H. Changes in floods and flood regimes in Canada. *Can. Water Res. J.* **41**, 139–150 (2016).
73. Dudley, R. W., Hodgkins, G. A., McHale, M. R., Kolian, M. J. & Renard, B. Trends in snowmelt-related streamflow timing in the conterminous United States. *J. Hydrol.* **547**, 208–221 (2017).
74. Burn, D. H. & Whitfield, P. H. Changes in flood events inferred from centennial length streamflow data records. *Adv. Water Res.* **121**, 333–349 (2018).
75. Kam, J., Knutson, T. R. & Milly, P. C. D. Climate model assessment of changes in winter–spring streamflow timing over North America. *J. Clim.* **31**, 5581–5593 (2018).

Additional information
Supplementary information The online version contains supplementary material available at https://doi.org/10.1038/s41586-024-07299-y.
Correspondence and requests for materials should be addressed to Yuting Yang.
Peer review information *Nature* thanks Ankur Dixit and the other, anonymous, reviewer(s) for their contribution to the peer review of this work. Peer reviewer reports are available.
**Reprints and permissions information** is available at http://www.nature.com/reprints.
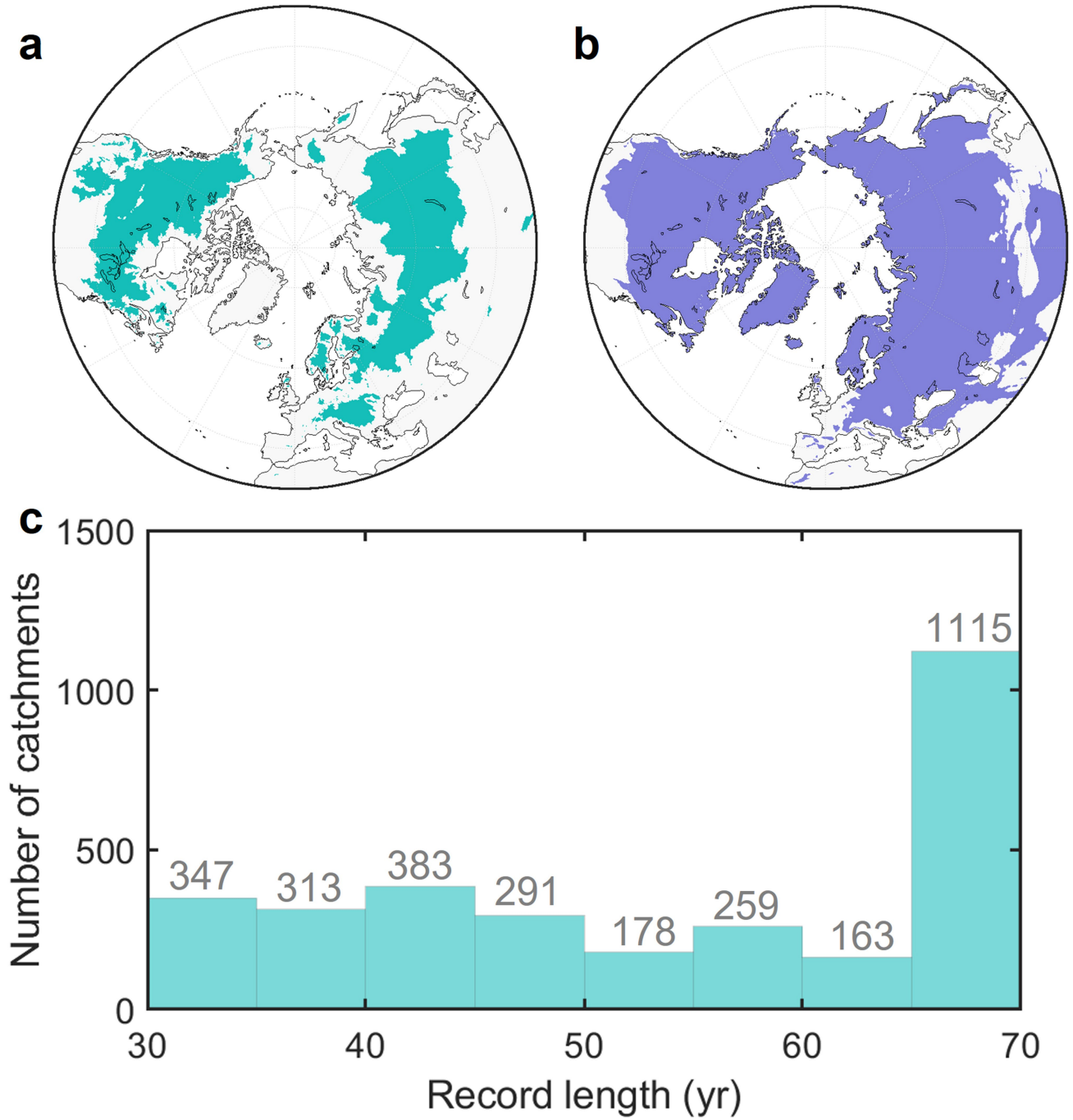
Extended Data Fig. 1 | Spatial and temporal coverages of the streamflow records. a | Spatial coverage of the 3049 catchments used herein. **b** | Spatial distribution of areas where the 1950–2020 mean annual snowfall fraction exceeded 0.1 over the Northern Hemisphere. **c** | Histogram of data length for the 3049 catchments. Numbers in **c** above each column indicate the count of catchments falling into each category.
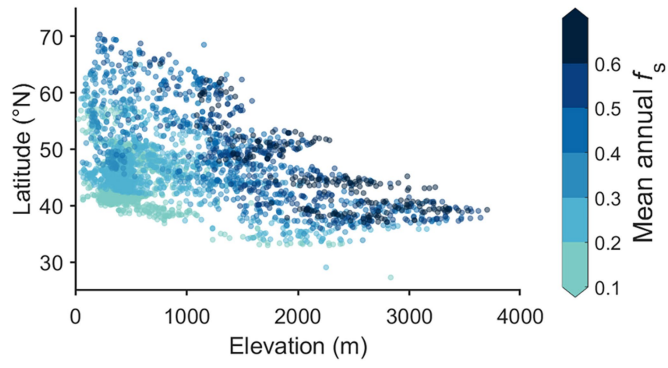
Extended Data Fig. 2 | Distribution of mean annual snowfall fraction in the elevation−latitude domain for the 3049 catchments.
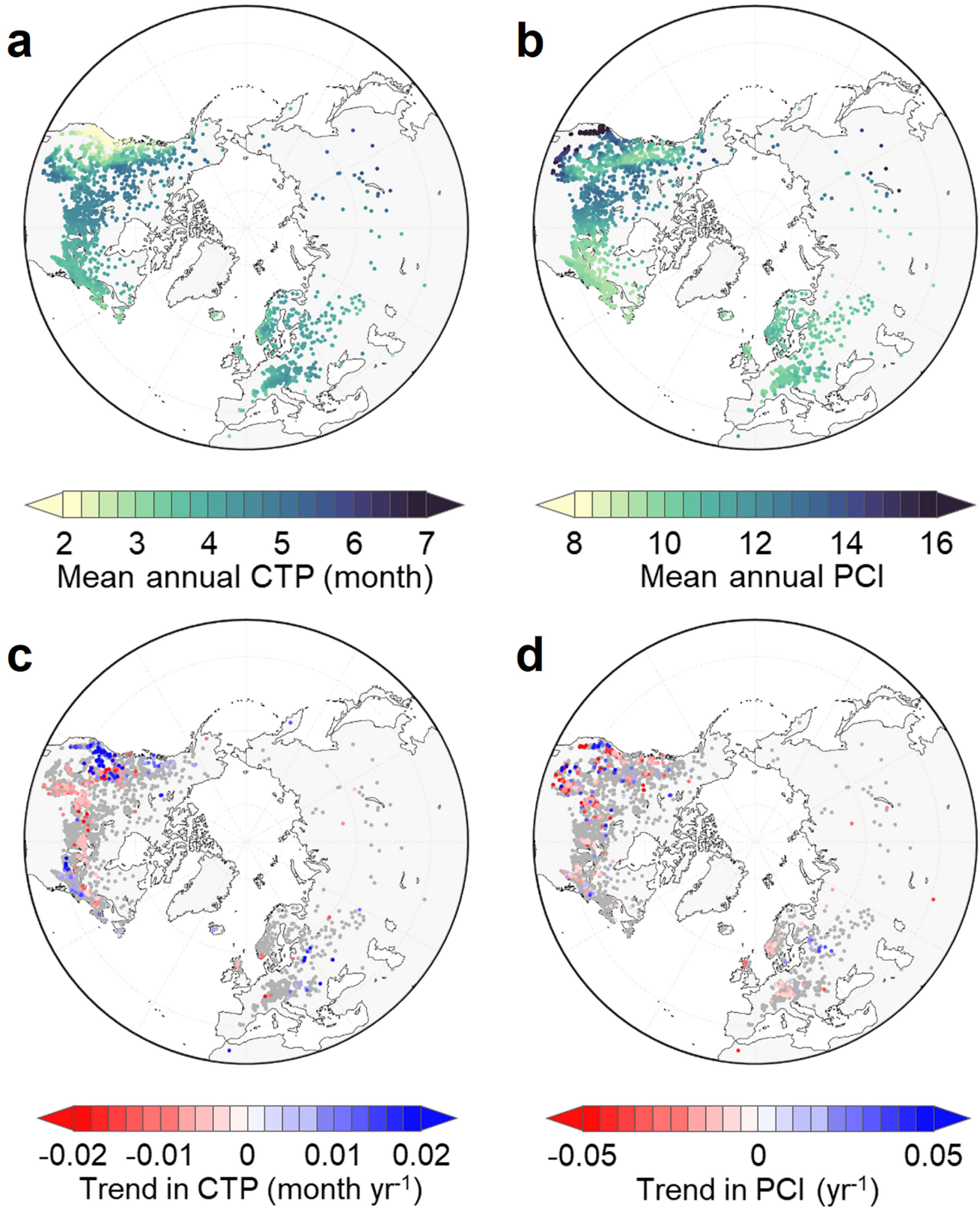
Extended Data Fig. 3 | Spatiotemporal patterns of precipitation seasonality across 3049 catchments over 1950–2020. a | Spatial distribution of mean annual precipitation timing (represented by the centre of mass of precipitation or CTP). **b** | Spatial distribution of mean annual seasonal precipitation variation (represented by PCI). **c** | Spatial distribution of trends in annual CTP. **d** | Spatial distribution of trends in annual PCI. In **c** and **d**, grey dots indicate that the trends are not statistically significant ($p > 0.1$, t-test).
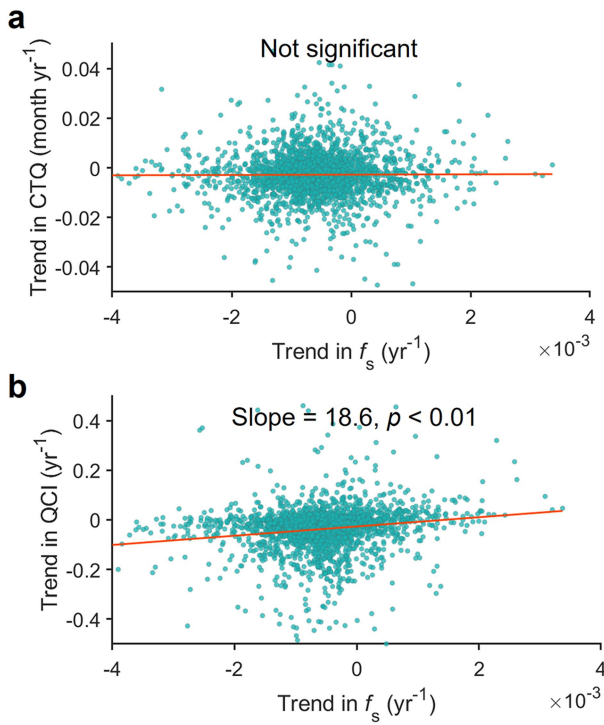
Extended Data Fig. 4 | Relationship between trends in snowfall fraction and streamflow seasonality across the 3049 catchments over 1950–2020. a |
Relationship between trends in snowfall fraction (f_s) and CTQ. **b |** Relationship between trends in f_s and QCI. The red solid lines show the best linear fits.

a

b
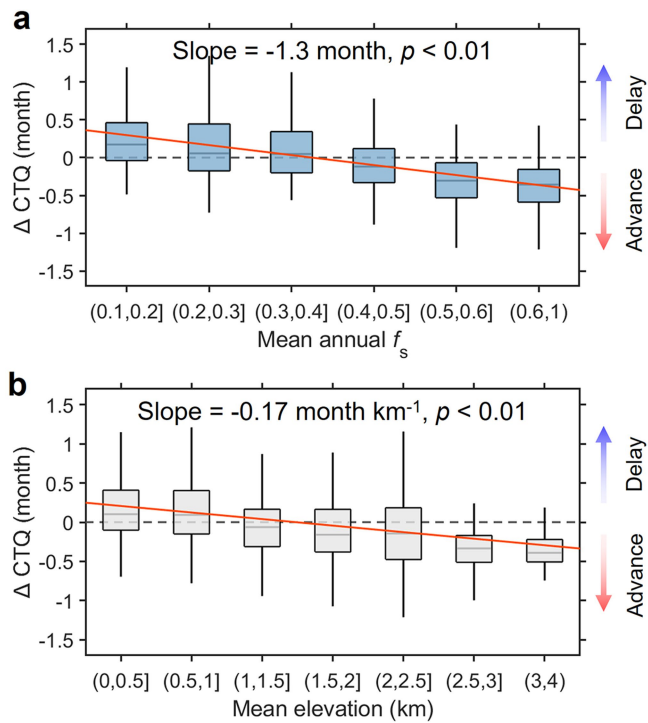
Extended Data Fig. 5 | Changes in streamflow timing between the two 10-year periods with the highest and lowest snowfall fraction. a | Changes in streamflow timing (ΔCTQ) as a function of mean annual snowfall fraction. **b** | ΔCTQ as a function of elevation. For each box, whiskers represent the 1st and 99th percentile, the top and bottom of the box are the 25th and 75th percentile and the median is represented by the horizontal line internal to the coloured box. The red solid line shows the best linear fit. The slopes of the linear regression models are quantified and the level of statistical significance is calculated using a *t*-test.
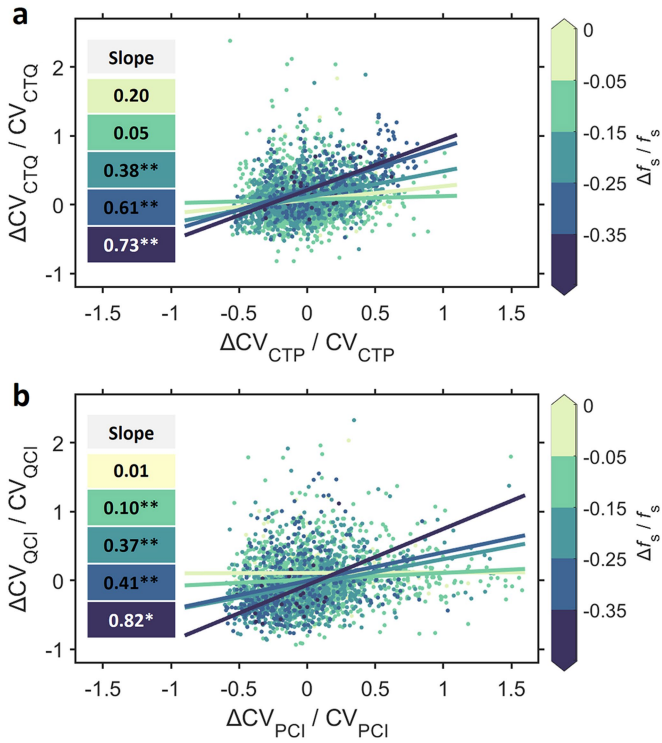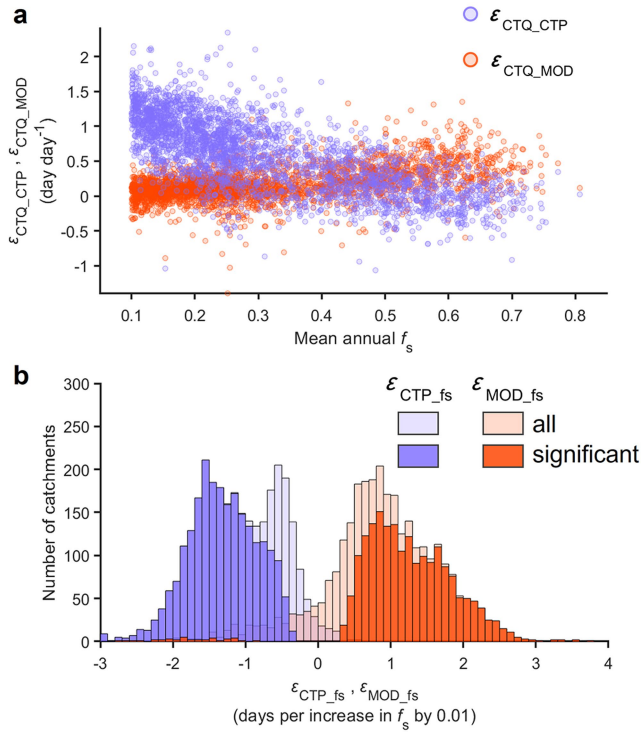
Extended Data Fig. 6 | Streamflow timing in response to changes in precipitation timing and snowmelt onset data. a | Sensitivities of CTQ to precipitation timing (ε_{CTQ_CTP}) and melt onset date (ε_{CTQ_MOD}) as a function of $\overline{f_s}$ for the 3049 catchments. **b** | Histogram of sensitivities of precipitation timing and melt onset date to declines in snowfall fraction (ε_{CTP_fs} and ε_{MOD_fs}) for the 3049 catchments. The snowmelt onset date (MOD) is determined following ref. 24, where MOD is calculated as the beginning of the first 5-day period during which snow water equivalent declined by more than 2.5 cm.
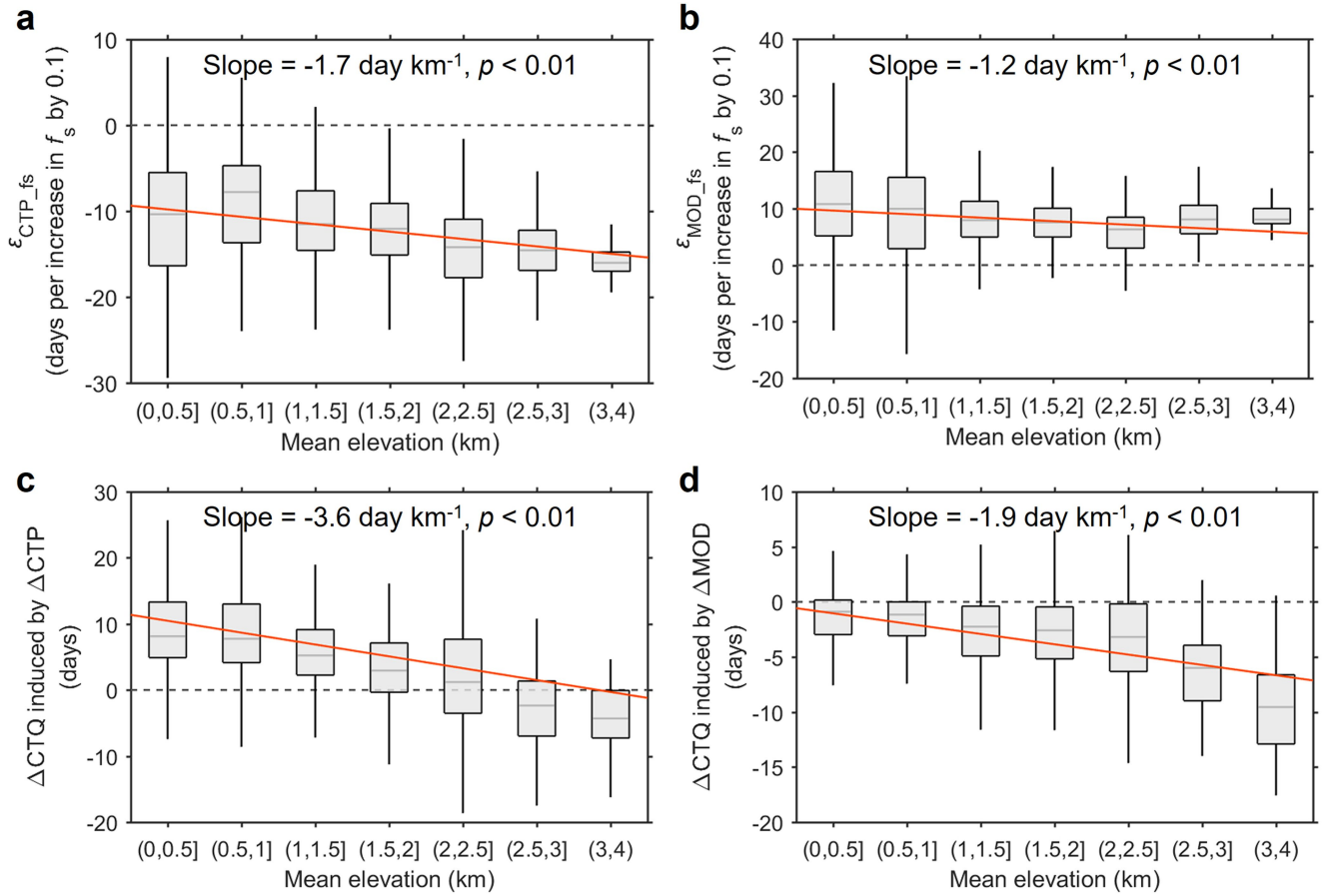
Extended Data Fig. 7 | Changes in seasonal streamflow and precipitation between low and high snowfall fraction periods. a-c | Number of catchments showing changes in (**a**) warm season streamflow, (**b**) cold season streamflow and (**c**) cold season precipitation. **d-f |** Relationship of changes in snowfall fraction (Δf_s) and changes in (**d**) warm season streamflow (ΔQ), (**e**) cold season streamflow (ΔQ) and (**f**) cold season precipitation (ΔP) between low- and high-f_s periods. In **d**, **e** and **f**, whiskers represent the 1st and 99th percentile, the top and bottom of the box are the 25th and 75th percentile and the median is represented by the horizontal line internal to the coloured box. The red solid lines show the best linear fits.

Extended Data Fig. 8 | Impact of changes in snowfall fraction on interannual variability of streamflow seasonality. a | Relationship of relative change in interannual variability of streamflow timing ($\Delta CV_{CTQ}/CV_{CTQ}$) and that of precipitation timing ($\Delta CV_{CTP}/CV_{CTP}$) between the two 20-year periods with the highest and lowest snowfall fraction (f_s). **b** | Relationship of relative change in interannual variability of streamflow seasonal variation ($\Delta CV_{QCI}/CV_{QCI}$) and that of precipitation seasonal variation ($\Delta CV_{PCI}/CV_{PCI}$) between two 20-year periods with the highest and lowest f_s. In both plots, catchments are divided into 5 groups based on their relative changes in f_s between the two 20-year periods and lines are the best linear fit across catchments in each group. The slopes of the linear regression models are presented in the inset, denoted by asterisks "*" and "**" to signify statistical significance at the 95% and 99% confidence levels (t-test), respectively.
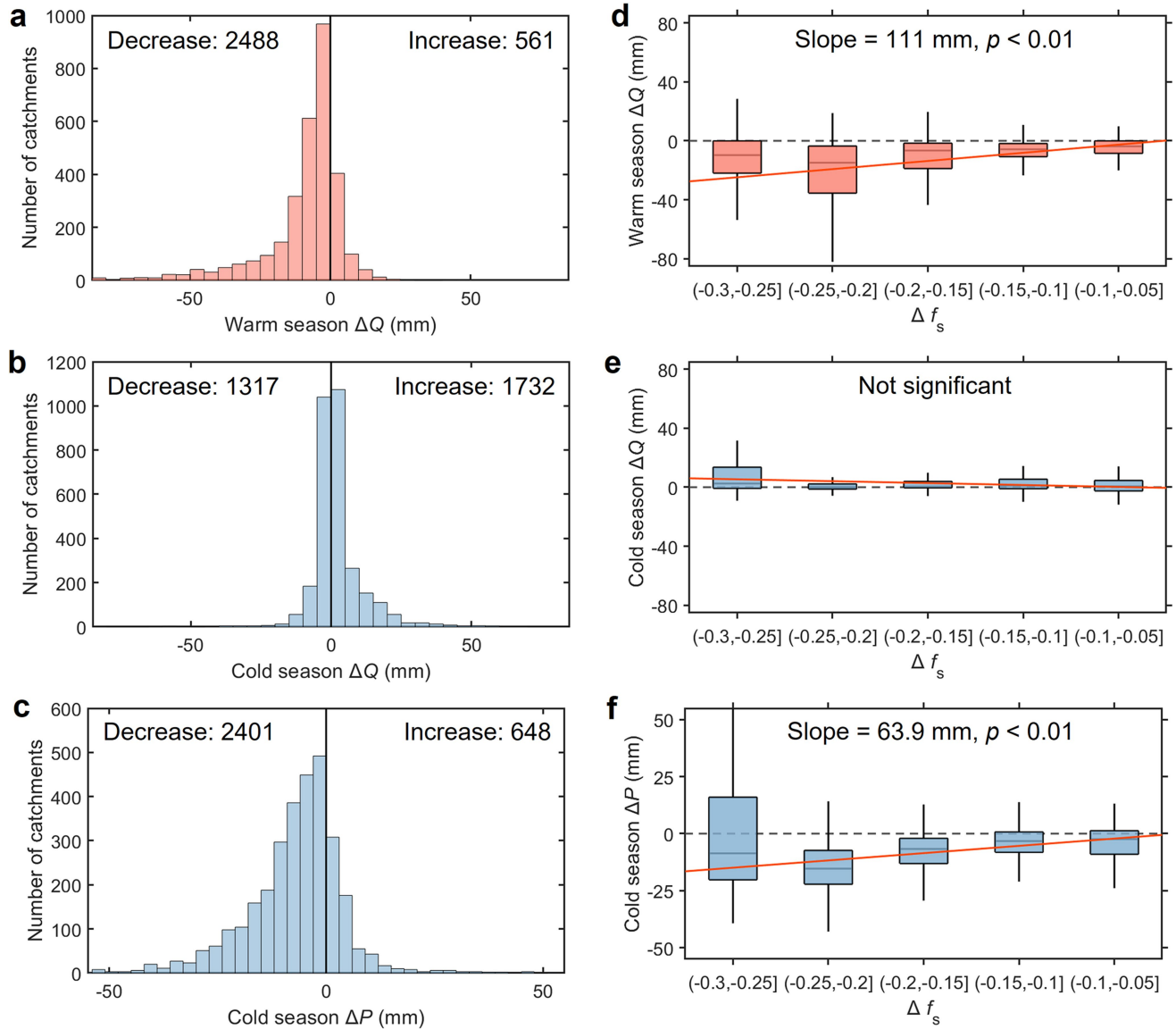
Extended Data Fig. 9 | Influence of temporal variations in snowfall fraction on streamflow timing along an elevation gradient for 3049 catchments. **a** | Elevation-dependent slopes in the linear regression between precipitation timing and snowfall fraction ($\varepsilon_{\text{CTP\_fs}}$) for the 3049 catchments. **b** | Elevation-dependent slopes in the linear regression between snowmelt timing and snowfall fraction ($\varepsilon_{\text{MOD\_fs}}$) for the 3049 catchments. **c** | Elevation-dependent changes in streamflow timing (ΔCTQ) resulting from alterations in precipitation timing (ΔCTP) between high- and low-f_s periods for the 3049 catchments. **d** | Elevation-dependent ΔCTQ induced by changes in snowmelt timing (ΔMOD) between high- and low-f_s periods for the 3049 catchments. For each box, whiskers represent the 1st and 99th percentile, the top and bottom of the box are the 25th and 75th percentile and the median is represented by the horizontal line internal to the coloured box. The red solid line shows the best linear fit.

Extended Data Table 1 | Overview of existing studies assessing changes in streamflow timing in snow-affected regions

Study	Region (Catchment number)	Area (km^2)	Period	Method	Key snow dynamic findings	Key Q timing findings
Ref. 5	western North America (362)	N/R	1948-2008	Obs	N/A	Variable changes (indicated by CTQ)
Ref. 7	western Canadian Arctic (1)	57	1985-2011	Obs	Earlier snowmelt	Later spring Q
Ref. 8	contiguous U.S. (97)	N/R	1957-2016	Obs	N/A	Earlier Q (indicated by CTQ)
Ref. 24	Colorado (1)	N/R	1978-2007	Obs	Earlier snowmelt	Earlier Q (indicated by CTQ)
Ref. 25	western U.S. (110)	N/R	1948-1994	Obs	Earlier snowmelt	Earlier spring Q
Ref. 26	western U.S. (175)	N/R	1951-2014	Model	Lower f_s	Earlier Q (indicated by CTQ)
Ref. 28	western U.S. (12)	126908	1913-1986	Obs	N/A	Earlier Q (no specific indicator used)
Ref. 29	western U.S. (84)	N/R	1950-2003	Obs	N/A	Earlier Q (indicated by CTQ)
Ref. 30	western North America (302)	N/R	1948-2002	Obs	Earlier snowmelt	Variable changes (indicated by CTQ)
Ref. 36	western U.S. (29)	30754	1962-2007	Obs	N/A	Variable changes (indicated by CTQ)
Ref. 37	western U.S. (1)	238	1962-2006	Obs	Lower f_s	Earlier Q (no specific indicator used)
Ref. 39	western U.S. (5)	N/R	1948-1991	Model	N/A	Earlier Q (no specific indicator used)
Ref. 55	western U.S. (4)	3170	1951-1980	Model	N/A	Earlier peak Q
Ref. 56	Colorado (3)	5228	N/R	Model	N/A	Earlier peak Q
Ref. 57	western U.S. (2)	1600	1949-1990	Model	N/A	Earlier Q (no specific indicator used)
Ref. 58	Siberian Lena (1)	2.43×10^6	1935-1999	Obs	Earlier snowmelt	Earlier peak Q
Ref. 59	western U.S. (3)	N/R	1900-2099	Model	Earlier snowmelt	Earlier peak Q
Ref. 60	European Alps (2)	3215	1981-2000	Model	Shorter snow cover duration	Earlier peak Q
Ref. 61	western U.S. (89)	N/R	1950-1999	Obs	Lower SWE	Earlier spring peak Q
Ref. 62	European Alps (5)	254	1981-2100	Model	N/A	Earlier peak Q
Ref. 63	eastern North America (179)	N/R	1913-2002	Obs	N/A	Variable changes (indicated by CTQ)
Ref. 64	western U.S. (4)	N/R	1916-2003	Model	Earlier snowmelt	Earlier Q (no specific indicator used)
Ref. 65	western U.S. (21)	N/R	1951-2005	Obs	N/A	Earlier Q (indicated by CTQ)
Ref. 66	Ob, Yenisei and Lena (3)	N/R	1988-2000	Obs	N/A	Earlier Q (no specific indicator used)
Ref. 67	northern Canada (26)	1.8×10^6	1915-2005	Obs	N/A	Variable changes (indicated by CTQ)
Ref. 68	western U.S. (7)	1×10^6	1950-1999	Model	Earlier snowmelt	Earlier Q (indicated by CTQ)
Ref. 69	western U.S. (8)	2385	N/R	Model	Lower SWE	Earlier annual minimum Q
Ref. 70	Spain (27)	N/R	1976-2008	Obs	Earlier snowmelt	Earlier Q (indicated by CTQ)
Ref. 71	Canada (280)	N/R	1931-2010	Obs	N/A	Mostly earlier peak Q
Ref. 72	western U.S. (75)	N/R	1920-2014	Obs	N/A	Earlier spring Q
Ref. 73	Canada and northern U.S. (27)	46482	1916-2015	Obs	N/A	Variable flood timing changes
Ref. 74	North American (303)	N/R	1933-2012	Model	N/A	Variable winter-spring Q timing changes
This study	Northern Hemisphere (3029)	2.13×10^7	1950-2020	Obs	Lower f_s & earlier snowmelt	Variable changes (indicated by CTQ)

Q: streamflow; CTQ: centre of mass of streamflow; SWE: snow water equivalent; f_s: snowfall fraction; Obs: observation. The current study is also included for comparison. "N/R" stands for 'not recorded' as a citable study area or study period was not recorded in the paper, whereas "N/A" denotes 'not applicable' as not all previous studies report snow dynamic findings[56-75].